Research Article

SOHAG JOURNAL OF SCIENCES

https://doi.org/10.21608/sjsci.2023.218544.1093

The Effect of Al and Sn Doping on the Optical and Electrical Properties of ZnO Nanostructures

G. Ahmed[1], M. F. Hasaneen[2,3], W. S. Mohamed[2,3], H.M. Ali[1], E.M.M. Ibrahim[1,*]

[1] *Physics Department, Faculty of Science, Sohag University, Sohag-82524, Egypt*
[2] *Physics Department, College of Science, Jouf University, Al-Jouf, Sakaka, P.O. Box 2014, Saudi Arabia*
[3] *Thin Films and Nanotechnology Lab, Physics Department, Faculty of Science, Sohag University, 82524, Sohag, Egypt*
[*] *E-mail: e.ibrahim@science.sohag.edu.eg*

Received: 11th July 2023, **Revised:** 5th September 2023, **Accepted:** 18th September 2023
Published online: 8th October 2023

Abstract: This work presents a comparison between the impact of Al and Sn doping on the structural, electrical, and optical properties of ZnO nanostructures (NSs). The samples have been synthesized using the well-known chemical vapor deposition at optimized conditions of temperature and ambient gas. The formation of the hexagonal Wurtzite structure of the ZnO has been confirmed using the x-ray diffraction technique. The impact of doping by Al and Sn on the morphology and particle shapes of ZnO has been explored using a field emission scanning electron microscope. The Kubelka-Munk's and Tauc's equations have been used for studying the optical properties while the Burstein Moss shift effect has been employed to explain the increase in the optical energy gap upon doping. The undoped and doped nanostructures show typical semiconductor features and the electrical conduction mechanisms have been described using Arrhenius's model.

Keywords: Nanostructures NSs, ZnO Nanostructures, Optical properties, Electrical conduction mechanisms

1. Introduction

Zinc Oxide is a direct wide band gap (≈3.37 eV) semiconductor with large binding energy (60 meV) [1-2]. It has gained a lot of interest due to many advantages such as non-toxicity, abundance, and high chemical and thermal stability. The possibility to tune the electrical and optical properties by doping makes ZnO feasible for fabricating many electronic devices [3]. Indeed, many elements including Co, Ni, Mn, S, In and Cu have been used as dopants for ZnO for tailoring the electrical and optical properties [4-11]. It was found that modulating the dopant type and concentration has a significant influence on the optoelectronic properties of ZnO. The defects formed by doping result in a significant variation in the structural, optical, and electrical properties of ZnO. For instance, Zn interstitials (Zn_i) and oxygen vacancies (V_o) act as donor defects leading to n-type behavior, while zinc vacancies (V_{Zn}) and oxygen interstitials (O_i) act as acceptors leading to p-type behavior [12]. It was observed that Al and Sn are promising candidates for tailoring the ZnO properties [13, 14]. Adding aluminum as a dopant reduces the crystallinity of ZnO but improves its electrical and optical properties [15, 16]. Also, it has been reported by Duan, et al. [14] that the incorporation of Sn in the ZnO lattice leads to a change in the morphology of ZnO nanocrystals from spherical to dumbbell-like shape with great enhancement in the near- and middle-infrared absorption which has been argued to the generation of localized surface plasmon resonance.

Many synthesis methods are employed to synthesize ZnO nanostructures including chemical vapor deposition (CVD), catalysis-driven molecular beam epitaxy, thermal evaporation, sonochemical method, and electrochemical deposition [12-16]. Among all, CVD is the most employed method where Zn or ZnO is evaporated in the hot zone (at temperature 900 – 1400 K) of a horizontal tube furnace reactor and then the gaseous phase precursors are pushed by a carrier gas to condense in a lower temperature zone forming the ZnO nanostructures. The synthesis conditions such as the hot zone and cold zone temperatures, gas flow rate, oxygen/carrier gas concentration, and catalyst type are valuable parameters used for controlling the morphology and the optoelectronic properties of the ZnO nanostructures.

Herein, ZnO, $Al_{0.04}Zn_{0.96}O$, and $Sn_{0.04}Zn_{0.96}O$ NSs are successfully synthesized by the chemical vapor deposition method. The structural, optical, and electrical properties are studied. The work aims to present a comparison between the effect of Al and Sn doping with a selected concentration on the structural, electrical, and optical properties of ZnO NSs. The selection of a specific concentration of the dopants was based on a series of experiments that showed particular variations of the corresponding properties.

2. Experimental details

2.1. Chemicals and synthesis process

$M_{0.04}Zn_{0.96}$ O (TM = Al or Sn) NSs were synthesized using the CVD method. Powders of Sigma-Aldrich Zn, Al, and Sn metals, (purity= 99.99%) were used as precursors. The precursors were weighed according to the required chemical stoichiometry, then mixed and ground thoroughly for 5 h. A suitable quantity of each mixture was put in a ceramic boat and placed in the horizontal quartz tube (36 cm in diameter and 60 cm in length) of a programmable tube furnace. The tube was

evacuated to ~2x10^{-3} Torr before starting Ar flow at a rate of 240 ml/min. After 1h of Ar flow, the temperature was increased gradually (with heating rate =10 ºC /min) to 880 ºC, and oxygen with a flow rate of 26 ml/min was introduced to the reactor by raising up the Ar gas flow rate to 300 ml/min. Deposition of white ZnO powder was observed inside the cold zone of the quartz tube (~40 cm from the hot zone center). The deposition process was continued for 30 min.

2.2. Characterization and measurement

The microstructural of the deposited materials was investigated by an x-ray diffractometer (Bruker D8-ADVANCE X-ray diffractometer) using Cu-Kα radiation (λ ≈ 1.54 Å). A field emission scanning electron microscope (FE-SEM) (Quanta 250 FEG) with an accelerating voltage of 30000V was used for studying the morphological features. To test the chemical stoichiometry, elemental analysis was carried out using the EDAX (Energy Dispersive Analyses of X-ray) technique. The optical properties of the samples were examined by a double ultraviolet/visible/near-infrared spectrophotometer (model; JASCO V-570). The electrical conductivity as a function of temperature (within a temperature range of 300–480 K) was measured using the two-probe method. The electrical terminals were connected to the sample surfaces with silver paste electrodes to achieve well electrical contact. The resistance was measured using digital millimeter type PROTEKA-445.

3. Results and Discussion:

3.1. Structural analysis:

XRD patterns of $Al_{0.04}Zn_{0.96}O$ and $Sn_{0.04}Zn_{0.96}O$ are illustrated in Fig. **1** in addition to the pattern of pure ZnO for comparison. The patterns depict the polycrystalline nature of the samples with typical hexagonal Wurtzite structure of ZnO (space group P63mc) in coincidence with JCPDS card number 04-008 - 8198 [17]. The planes (100), (002), (101), (012), (110), (013), (200), (112), (201), (004), and (202) appear as the favorable orientation directions of the crystal growth [18]. The sharpness of the peaks indicates the good crystallinity of the samples under study. No secondary Al-, Sn- Zn-based, or other impurity phases could be observed indicating that the Al and Sn atoms substitute Zn atoms without a change in the crystal structure of ZnO. This observation agrees with other previously published works where the hexagonal Wurtzite lattice of ZnO was stable and didn't change with dopants as long as the dopant concentration was below the solubility limit in the ZnO matrix [**14, 19, 20**]. Also, ionic radii of Sn^{+4} (~69 pm) and Al^{+3} (~50 pm) are lower than that of Zn^{+2} (~74 pm) which makes the substation process likely to occur [**21,22**].

The XRD data allows us to calculate the crystallite size (D), lattice strain (ε), and dislocations (δ) using the following relations and tabulated in Table **1**.

$$\varepsilon = \frac{\beta}{4\tan(\theta)} \rightarrow \quad (1)$$

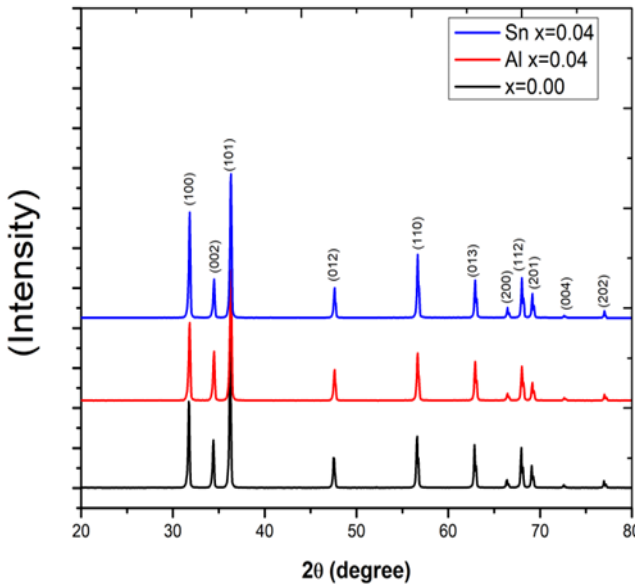

Fig. 1: XRD pattern of prepared pure ZnO and Al-doped, Sn-doped nanostructures.

$$D = \frac{k\lambda}{\beta\cos(\theta) - 4\,sign(\theta)} \rightarrow \quad (2)$$

$$\delta = \frac{n}{D^2} \rightarrow \quad (3)$$

where θ is Bragg's angle, λ is the incident ray wavelength, n is a constant usually close to unity, K is the shape factor taken to be 0.89 and β is the full width at half maximum (FWHM) of the XRD peak. The data tabulated in Table **1** reveal that the incorporation of Al, or Sn decreases the crystallite size but increases the lattice strain and lattice dislocations which can be attributed to the small radii of Sn^{+4} and Al^{+3} compared to the radius of Zn^{+2} ion [21].

3.2. Morphological and elemental analyses:

Fig. **2** illustrates the FE-SEM images of the samples. Generally, the data reveal that all samples consist of nanostructures and the dopant type has a significant impact on the ZnO morphology. As seen in Fig. **2a**, pure ZnO consists of randomly shaped nanoflakes (NFs) with approximately 130 nm in thickness with width and length that can reach a few micrometers. The growth of ZnO NSs is explained by the catalyst-free Vapor-solid (VS) model in our previous work [**12**]. $Al_{0.04}Zn_{0.96}O$ sample.

(Fig **2.b)** reveals a significant change from nanoflakes-like to nanowires (NWs) shape decorated with nanoparticles on the surface. The NWs have an average diameter of ~100 nm and a length of several micrometers. However, doping with Sn enlarges the NFs thickness to reach about 150 mm with the growth of small needle-like shape NSs (Fig. **2c**). EDX spectra (Fig. **2d-e**) show that all of the synthesized samples are of high purity and coincide with the desired chemical stoichiometry.

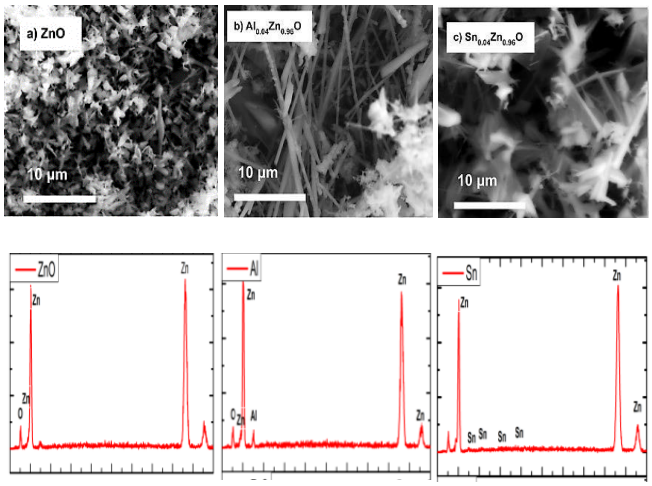

Fig. 2: FE-SEM images of a) pure ZnO, b) $Al_{0.04}Zn_{0.96}O$, and c) $Sn_{0.04}Zn_{0.94}O$ NSs. EDX spectra of d) pure ZnO, e) $Al_{0.04}Zn_{0.96}O$, and f) $Sn_{0.04}Zn_{0.96}O$ NSs.

Table 1: Lattice parameters, optical band gap, and electrical activation energies of Al-, Sn-doped, and pure ZnO NSs

Doping	Crystallite size (D) nm	Lattice strain $\varepsilon x10^{-4}$	Lattice dislocations δ $x10^{-5}$	Optical band Gap E_g eV	Electrical conductivity at 393K $Ohm^{-1}m^{-1}$	High temperature activation Energy E_{ah} eV	Low temperature activation Energy E_{al} eV
Pure ZnO	52.2±1.3	2.6±0.07	36.6±0.9	3.30	$7.16x10^{-4}$	0.48	0.114
$Al_{0.04}Zn_{0.96}O$	44.6±1.1	3.1±0.08	50.1±1.2	3.26	$6.73x10^{-6}$	0.36	0.08
$Sn_{0.04}Zn_{0.96}O$	48.8±1.2	2.8±0.07	41.9±1	3.24	$4.5x10^{-5}$	0.18	----

3.3 Optical analysis:

The optical properties of the synthesized samples were investigated by recording the diffused reflectance spectra (not included here). The Kubelka-Munk function (F(R)) converts the reflectance (R) into the absorption coefficient through the relation:

$$F(R) = \frac{(1-R)^2}{2R} = \frac{k}{s} \rightarrow \quad (4)$$

where S and K are the scattering Kubelka-Munk and absorption coefficients, respectively [9]. The Kubelka-Munk function F(R) is related to the absorption coefficient α as:

$$K = 2\alpha = SF(R) \rightarrow \quad (5)$$

The optical band gap E_g can be determined from Tauc's equation as follows:

$$F(R)h\nu = \beta_1(h\nu - E_g)^m \rightarrow \quad (6)$$

where hν is the photon energy; E_g is the optical energy gap, m is an index that equal 1/2 for ZnO as a direct band gap semiconductor and β1 is a constant. Tauc's equation allows determining E_g using $[F(R)\ h\nu)]^{1/2}$ vs. hν plots shown in Fig. 3. The data reveals that the pure ZnO nanoflakes have E_g = 3.23 eV which is slightly lower than the value (3.3 eV) reported for ZnO single crystal. Noteworthy, the energy band gape is significantly influenced by many factors such as growth stress, quantum confinement and structural defects [11]. Adding Al increases the E_g value to 3.26 eV. This value is comparable to that reported by Norouzzadeh et al. (3.18 eV) [23] and Khlayboonme and Thowladda (3.24 eV) [23] for the ZnO nanoparticles synthesized by the Sol-gel method. Similarly, doping with Sn increases the E_g value of ZnO to 3.3 eV. In comparison with other published data, E_g of our Sn-doped ZnO nanoflakes is higher than that reported by Roguai and Djelloul [24] for Sn-doped ZnO synthesized using pneumatic spray pyrolysis technique (2.96 eV). The increase in the E_g value with Al and Sn doping agrees with other previously reported results [25,26] and can be attributed to two reasons: i) creation of degenerate energy levels (Burstein Moss shift effect) with doping that causes movement of the Fermi level above the conduction band edge and thus increases the band gap [27, 28]. ii) The increase in the strain and dislocation content revealed by the XRD results which alters the electronic structure [29, 30].

3.4. Electrical properties:

Fig. 4a shows the electrical resistivity (ρ) vs. temperature (T) plots of the samples under study. The data reveal thermally activated semiconducting features that ρ decreases as the temperature increases indicating that more charge carriers overcome the energy barrier by heating and contribute to the electrical conduction [31]. It was found that the temperature dependency of the electrical resistivity is well represented by Arrhenius's equation:

$$\rho = \rho_0 \exp\left(\frac{E_a}{K_B T}\right) \rightarrow \quad (7)$$

where ρ_0 is the pre-exponential factor, K_B is the Boltzmann's constant, E_a is the activation energy of the electrical conduction.

The linearity of the Ln(ρ) versus 1000/T plots illustrated in Fig. 4b confirms the good fitting of the results with the Arrhenius equation. Since each of the Ln(ρ) vs. 1000/T plots of pure ZnO and Al-doped samples shows two distinct straight lines with different slopes, the electrical conduction in the samples is described by two different mechanisms with two activation energies (herein denoted by E_{ah} and E_{al}, in the high and low-temperature ranges, respectively). E_{ah} = 0.48 and 0.36 eV and E_{al} = 0.114 and 0.08 were determined for undoped and Al-doped ZnO samples, respectively. However, the Ln (ρ) vs. 1000/T plot of Sn-doped ZnO sample is in one straight line indicating domination of one conduction mechanism with one value of the activation energy (herein denoted by E_a) over the whole temperature range of measurement. The E_a value of the

Sn-doped sample was calculated to be 0.18 eV. The decrease in the activation energy values by Al doping is due to the charge carriers that are created by replacing Zn^{2+} by Al^{3+} ions in the lattice. The appearance of one conduction mechanism of the Sn-doped sample may be attributed to the abundance of the free charge carriers created by the substitution of Zn^{2+} by Sn^{4+} compared to the case of Al^{3+}. Noteworthy, Al, and Sn are acting as donors in the ZnO sample. The activation energy values of the samples under study are close to those reported in other literature [29].

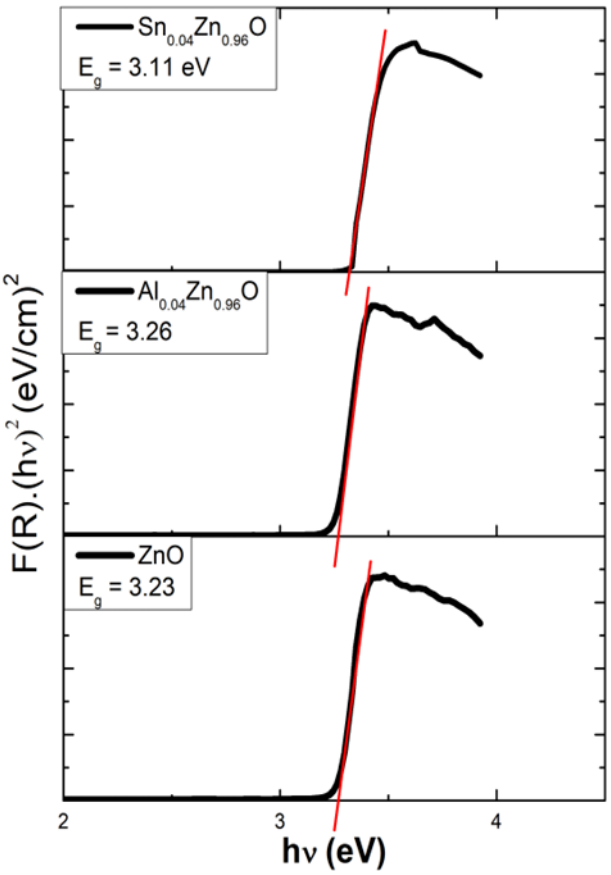

Fig. 3: $[F(R)h\nu)]^{1/2}$ vs. hν plots for pure ZnO, $Al_{0.04}Zn_{0.96}O$ and $Sn_{0.04}Zn_{0.94}O$ NSs

4. Conclusion

Undoped, Al- and Sn-doped ZnO nanostructures are successfully synthesized using the chemical vapor deposition method. The NSs are well crystalized in a typical hexagonal Wurtzite structure. Type of the doping element has a significant impact on the sample morphology and particle shape. Chemical vapor deposition is a reliable route for successful replacement of the Zn atoms by Al and Sn atoms in the ZnO lattice. Doping with Al or Sn creates degenerate energy levels and increases the crystalline strain and dislocations content which in turn increases the optical energy gap of ZnO NSs. Electrically, the undoped ZnO and Al-doped ZnO NSs show two conduction mechanisms upon elevating the ambient temperature. However, Sn-doped ZnO NSs are characterized by one conduction mechanism showing one value of the activation energy over the whole temperature of measurement. The results present the doping process as a valuable tool for tailoring the electrical and optical properties of ZnO to maximize its utility in various optoelectronic devices.

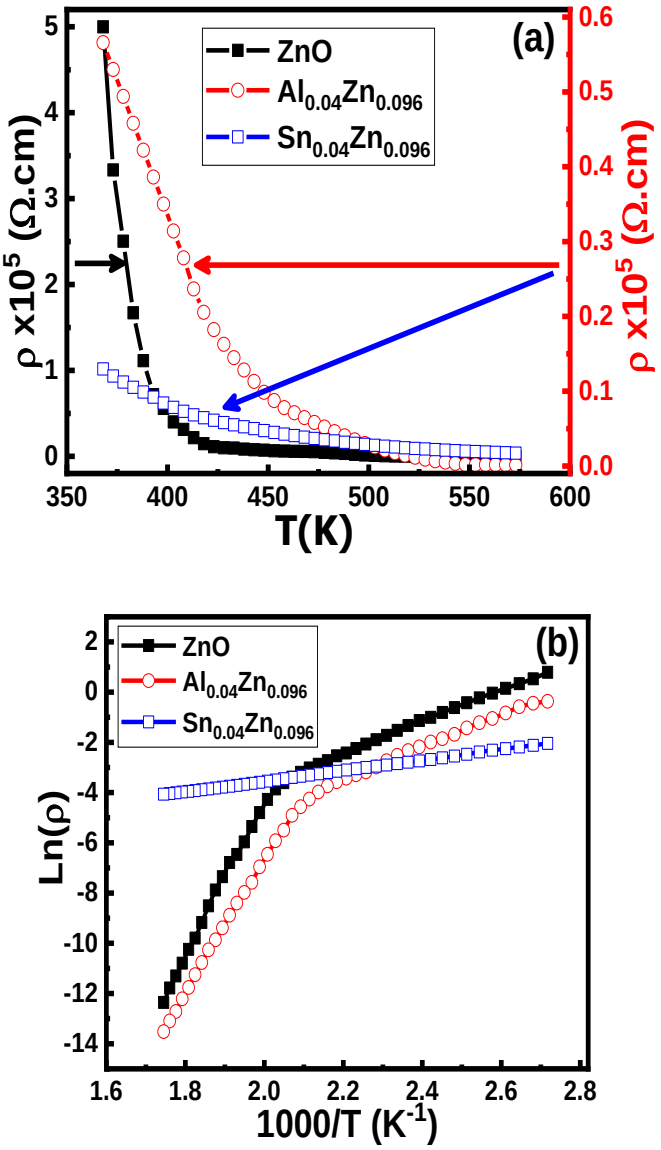

Fig. 4: (a) electrical resistivity (ρ) vs. temperature (T) and b) Ln (ρ) vs. 1000/T plots of ZnO, $Al_{0.04}Zn_{0.96}O$ and $Sn_{0.04}Zn_{0.96}O$ NSs.

CRediT authorship contribution statement:

G. Ahmed: Sample synthesis and characterization, analyses, calculations, writing the original draft, and data presentation. M. F. Hasaneen: Optical measurements and

data analyses. W. S. Mohamed: Writing - Review & Editing, investigation. H.M. Ali: Supervision, resources, methodology. E.M.M. Ibrahim: main supervision, writing - Review & Editing, Project administration.

Data availability statement

The data used to support the findings of this study are available from the corresponding author upon request.

Declaration of competing interest

The authors declare that they have no known competing financial interests or personal relationships that could have appeared to influence the work reported in this paper.

References

[1]. A. A. EL-Fadl, G. A. Mohamed, A. B. Abd EL-Moiz, M. Roshad, Physica B: Condensed Matter 366 (2005) 44-54.
[2]. Prakash, T., Jayaprakash, R., Espro, C. et al. J Mater Sci 49, (2014) 1776–1784.
[3]. Sato Y, Yamamoto T. J Am Ceram Soc 90 (2007) 337–357
[4]. A. Sedky, N. Afify, Abdullah Almohammedi, E.M.M. Ibrahim, Atif Mossad Ali, Optical and Quantum Electronics 55 (2023) 456
[5]. E. M. M. Ibrahim, A. Z. Mahmoud, L. Galal, Y. El Sayed, E. R. Shaabang, Journal of Ovonic Research, 17 (2021) 519 – 532.
[6]. H. Ali, A.M. Alsmadi, B. Salameh, M. Mathai, M. Shatnawi, N.M.A. Hadia, E.M.M. Ibrahim, Journal of Alloys and Compounds 816 (2020) 152538
[7]. A. A. Othman, M. A. Osman, Manar A. Ali, W. S. Mohamed, E. M. M. Ibrahim, Journal of Materials Science: Materials in Electronics 31 (2020) 1752–1767.
[8]. A.A. Othman, M.A. Osman, E.M.M. Ibrahim, Manar A. Ali, A.G. Abd-Elrahim, Materials Science and Engineering B 219 (2017) 1–9.
[9]. A.A. Othman, Manar A. Ali, E.M.M. Ibrahim, M.A. Osman, Journal of Alloys and Compounds 683 (2016) 399-411.
[10]. Madeha Ahmed Awad, Eslam Mohamed Mohamed Ibrahim, and Ahmed Mohamed Ahmed. The European Physical Journal Applied Physics 72 (2015) 30303
[11]. M. A. Awad, A. M. Ahmed, V. O. Khavrus, E.M.M. Ibrahim, Ceramics International, 41 (2015) 10116-10124.
[12]. G. Ahmed, W.S. Mohamed, M.F. Hasaneen, H.M. Ali, E.M.M. Ibrahim, Optical Materials 140 (2023) 113880.
[13]. Gordon, R.G. Criteria for Choosing Transparent Conductors. MRS Bulletin 25, (2000) 52–57.
[14]. Min Duan, JingWang, Chao Liu, Jun Xie, Jianjun Han, Journal of Non-Crystalline Solids 459 (2017) 32–35.
[15]. M.W. Zhu, H.B. Ma, P.H. Jin, et al. Appl. Phys. A 126 (2020) 484.
[16]. O. Urper, N. Baydogan, J. Mater. Lett. 258 (2020) 126641.
[17]. S. Johnson Jeyakumar, J. Vasudevan, B. Arunkumar, M. Jothibas, A. Rajeswari, R. Sathiskumar, A. Muthuvel. Materials Today: Proceedings,Geurts, 48, 2, (2022) 371-376
[18]. J. (2010). Crystal Structure, Chemical Binding, and Lattice Properties. In: Zinc Oxide. Springer Series in Materials Science, vol 120. Springer, Berlin, Heidelberg.
[19]. Haseman, M.S., Saadatkia, P., Warfield, J.T. et al. J. Electron. Mater. 47, (2018) 1497–1504
[20]. Akhiruddin, N., Muhammad, R., Wahab, Y., & Ibrahim, Z. In Solid State Phenomena 268, (2017) 249–253.
[21]. Kohei Nishimura, Daisuke Hirotani, Muhammad Akmal Kamarudin, Qing Shen, Taro Toyoda, Satoshi Iikubo, Takashi Minemoto, Kenji Yoshino, and Shuzi Hayase, ACS Applied Materials & Interfaces 11 (34), (2019) 31105-31110.
[22]. P. Norouzzadeh, Kh. Mabhouti, M.M. Golzan, R. Naderali, J. Optik 204 (2020) 164227.
[23]. S. T. Khlayboonme and W. Thowladda, J. Mater. Res. Express 8 (2021) 076402
[24]. Bedia, F. Z., Bedia, A., Aillerie, M., Maloufi, N., & Benyoucef, B. In Energy Procedia 74, (2015) 539–546.
[25]. E. Burstein, Anomalous optical absorption limit in InSb, Phys. Rev, 93 (1954) 632.
[26]. Kim, C. E., Moon, P., Kim, S., Myoung, J. M., Jang, H. W., Bang, J., & Yun, I. In Thin Solid Films 518, (2010) 6304–6307.
[27]. N.R. Yogamalai, A.C. Bose, J. Solid Chem. 184 (2011) 12-20.
[28]. M. Wakaki, K. Kudo, T. Shibuya, Physical Properties and Data of Optical Materials, CRC Press, New York, 2007.
[29]. Ilican S., Caglar Y., Caglar M., Yakuphanoglu F., Physica E: Low-Dimensional Systems and Nanostructures, 35 (1) (2006) 131-138.
[30]. Zak A.K., Abrishami M.E., Majid W.H.A., Yousefi R., Hosseini S.M. Ceramics International, 37 (1) (2011) 393-398.
[31]. S Tipawan Khlayboonme, Warawoot Thowladda, 2021 Mater. Res. Express 8 076402.